

Evidence of Ising pairing in superconducting NbSe₂ atomic layers

Xiaoxiang Xi^{1*}, Zefang Wang^{1*}, Weiwei Zhao¹, Ju-Hyun Park², Kam Tuen Law³,
Helmuth Berger⁴, László Forró⁴, Jie Shan^{1δ}, and Kin Fai Mak^{1δ}

¹Department of Physics, The Pennsylvania State University, University Park,
Pennsylvania 16802-6300, USA

²National High Magnetic Field Laboratory, Florida State University, Tallahassee,
Florida 32310, USA

³Department of Physics, Hong Kong University of Science and Technology, Clear
Water Bay, Hong Kong, China

⁴Institute of Condensed Matter Physics, Ecole Polytechnique Fédérale de Lausanne,
1015 Lausanne, Switzerland

*These authors contributed equally to this work.

δCorrespondence to: jus59@psu.edu, kzm11@psu.edu

Two-dimensional transition metal dichalcogenides with strong spin-orbit interactions and valley-dependent Berry curvature effects have attracted tremendous recent interests¹⁻⁷. Although novel single-particle and excitonic phenomena related to spin-valley coupling have been extensively studied^{1,3-6}, effects of spin-momentum locking on collective quantum phenomena remain unexplored. Here we report an observation of superconducting monolayer NbSe₂ with an in-plane upper critical field over six times of the Pauli paramagnetic limit by magneto-transport measurements. The effect can be understood in terms of the competing Zeeman effect and large intrinsic spin-orbit interactions in non-centrosymmetric NbSe₂ monolayers, where the electronic spin is locked to the out-of-plane direction. Our results provide a strong evidence of unconventional Ising pairing protected by spin-momentum locking and open up a new avenue for studies of non-centrosymmetric superconductivity with unique spin and valley degrees of freedom in the exact two-dimensional limit.

Monolayer transition metal dichalcogenide (TMD) of the hexagonal structure consists of a layer of transition metal atoms sandwiched between two layers of chalcogen atoms in the trigonal prismatic structure⁸ (Fig. 1a). It possesses out-of-plane mirror symmetry and in-plane inversion asymmetry. The presence of the transition metal also gives rise to large spin-orbit interactions (SOIs). The mirror symmetry restricts the crystal field ($\vec{\epsilon}$) to the plane. The SOIs split the spin states at finite momentum \vec{k} in the absence of inversion symmetry. They manifest as an effective magnetic field along the direction of $\vec{k} \times \vec{\epsilon}$, which is out-of-plane for the restricted two-dimensional (2D) motion of electrons in the plane. The electronic spin is thus oriented in the out-of-plane direction and in opposite directions for electrons of opposite momenta¹⁻³ (Fig. 1a). Such spin-momentum locking is destroyed in the bulk where inversion symmetry and spin degeneracy are restored^{1,2,7} (Fig. 1b). Novel valley- and spin-dependent phenomena including optical orientation of the valley polarization^{3,4} and the valley Hall effect⁵ arisen from spin-momentum locking have been recently demonstrated in group-VI TMD

monolayers such as MoS₂. The effect of spin-momentum locking on collective quantum phenomena, however, remains experimentally unexplored.

In this work, we demonstrate very high in-plane upper critical fields induced by spin-momentum locking in *superconducting monolayers* of group-V TMD niobium diselenide (NbSe₂). This was achieved through transport and magneto-transport studies of high quality NbSe₂ devices of varying layer thickness. Bulk 2H-NbSe₂ is a well-studied type II anisotropic multiband superconductor with a zero-field critical temperature $T_{C0} \approx 7 \text{ K}^{9-14}$. Superconductivity in atomically thin NbSe₂^{15,16} down to the monolayer thickness¹⁷ has also been observed recently. Monolayer NbSe₂ can be viewed as heavily hole doped monolayer MoSe₂^{8,18}. The Fermi surface is composed of one pocket at the Γ point and two pockets at the K and the K' points of the Brillouin zone with each pocket spin split into two pockets by the SOIs¹⁸ (Fig. 1a); The spin splitting at the Γ point is much smaller than that at the K (K') point¹⁸ and the spin-momentum locking effects are dominated by the K (K') pockets.

In conventional superconductors, superconductivity can be quenched under a sufficiently high external magnetic field by the orbital^{11,19} and spin effect^{20,21}, which are originated, respectively, from the coupling between the electron momentum and the magnetic field (e.g. vortex formation) and from spin alignment by the magnetic field. In the limit of monolayer thickness, the interlayer coupling vanishes and the orbital effect is absent for an in-plane magnetic field H_{\parallel} . The in-plane upper critical field (critical field at zero temperature) H_{c20}^{\parallel} is determined by direct spin-flip, known as the Pauli paramagnetic limit $H_P \approx 1.84 T_{C0}$ (in Tesla for T_{C0} in Kelvin) for isotropic BCS superconductors^{20,21}. Under this field the Zeeman splitting energy matches the superconducting energy gap, or equivalently, the binding energy of a Cooper pair. Spin-momentum locking and the consequent pairing of the K and K' electrons with spin locked to the two opposite out-of-plane directions (Fig. 1a), referred to as *Ising pairing*, is expected to enhance H_{c20}^{\parallel} significantly above the Pauli limit H_P in monolayer NbSe₂.

In our experiment, we fabricated monolayer and few-layer samples of NbSe₂ by mechanical exfoliation of 2H-NbSe₂ single crystals followed by direct transfer onto SiO₂/Si substrates with pre-patterned electrodes and encapsulation by thin layers of hexagonal boron nitride (see Methods). The sample thickness was determined with monolayer accuracy by optical spectroscopy, particularly, the frequency shift of the interlayer shear mode¹⁷. The crystal symmetry is characterized by optical second harmonic generation. (See Supplementary Materials Section 1 for details on optical characterization). Figure 1c is an optical image of a representative device (bilayer in this case). The temperature dependence of the normalized four-point resistance $R(T)/R(300 \text{ K})$ at zero magnetic field is shown in figure 1d from 2 – 300 K for a typical bulk, bilayer and monolayer device. (See Supplementary Materials Section 2 for original data and more devices). All samples show a metallic behavior with phonon-limited transport at high temperature (with $R \propto T$) and disorder-limited transport at low temperature (with R approaching a constant value) before reaching the superconducting state. The residual resistance ratio (RRR) evaluated using the room temperature resistance and the normal state resistance right above the superconducting transition R_n (taken at 8 K) varies from ~

30 in the bulk to ~ 10 in the monolayer device. The square resistance per layer (at 8 K) was calculated to be $\approx 200 \Omega$ for the bilayer (which has a good geometry) and similar values were estimated for other devices. These values are much smaller than $\frac{h}{4e^2} \approx 6450 \Omega$, where a disorder-induced superconductor-insulator transition emerges²². Here e is the electron charge and h is the Planck constant. Our samples are therefore in the low disorder regime compared to similar layered compounds studied previously¹⁶ and the disorder effects on T_{C0} are expected to be small²².

Figure 2a shows the temperature dependence near the transition of the resistance normalized by R_n for NbSe₂ samples of varying thickness N . Superconductivity is observed for all samples down to the monolayer thickness. A significant drop in the transition temperature accompanied with a significant broadening is observed for $N < 4$ (~ 2.68 nm). The broadening can be attributed to enhanced thermal fluctuations in 2D^{19,23} when the sample thickness falls below the bulk out-of-plane coherence length of 2.7 nm¹⁰. We have used the Aslamozov-Larkin formula²⁴ to determine T_{C0} (solid lines, Fig. 2a), which is close to the temperature corresponding to $0.5R_n$. We have also performed current excitation measurements to investigate the importance of phase fluctuations, and the Berenzinskii-Kosterlitz-Thouless transition temperature²³ is found to be close to $T(0.01R_n)$. Figure 2b summarizes the N -dependence of T_{C0} , $T(0.5R_n)$ and $T(0.01R_n)$. The monotonic dependence of T_{C0} on N can be accounted for by the decreasing interlayer Cooper pairing^{25,26} (the linear dependence of $[\ln \frac{T_{C0}(N)}{T_{C0}(N=1)}]^{-1}$ on $[\cos(\frac{\pi}{N+1})]^{-1}$ in the inset of Fig. 2b). Effects on T_{C0} from the competing charge-density-wave order that is enhanced with decreasing N are thus likely to be weak in NbSe₂¹⁴. (See Supplementary Materials Section 3 and 4 for details on the study of the characteristics of 2D superconductivity in NbSe₂).

With the above understanding of the nature of superconductivity in 2D NbSe₂, we now study its magnetic response. Figure 3a-c show the temperature dependence of the four-point resistance for a bulk, trilayer and monolayer sample under both out-of-plane (H_{\perp}) and in-plane magnetic fields (H_{\parallel}). A second monolayer device with two-point measurements up to 20 T is also included. For all samples, we normalize the temperature by the corresponding T_{C0} , and the resistance by R_n . We define the critical temperature T_C under a finite magnetic field H_{c2} as the temperature corresponding to 50% of R_n , in accordance with the zero field convention. For two-point measurements, as shown in Fig. 3c, we assign T_{C0} as the temperature at which a rapid resistance drop occurs while the sample is cooled from the normal state. It is clear that for all samples superconductivity is more susceptible to H_{\perp} than to H_{\parallel} and the magnetic anisotropy is significantly larger in atomically thin samples than in the bulk. (For angular dependence study of the magnetic response refer to Supplementary Materials Section 5).

We summarize the $H_{c2} - T_C$ phase diagram for differing sample thickness N in figure 4 for both H_{\perp} (open symbols) and H_{\parallel} (filled symbols). For comparison, we normalize the critical field H_{c2} by the BCS Pauli paramagnetic limit H_P and the critical temperature T_C by T_{C0} for each sample. For out-of-plane fields, our experiment shows a linear $H_{c2}^{\perp} - T_C$ dependence that is largely thickness independent. The result can be

explained by considering the orbital effect, i.e. overlaps of vortex cores, as the major quenching mechanism. H_{c20}^\perp is determined by the combined effect of in-plane coherence length and transport mean free path¹⁹. While the coherence length increases with reducing thickness (because of the reduction in T_{C0}), the mean free path decreases as the material becomes more disordered. The net effect is a weak $H_{c2}^\perp - T_C$ dependence on N . The measured upper critical field $H_{c20}^\perp \approx 4$ T ($\ll H_P$) agrees well with the value reported for bulk NbSe₂^{9,10}.

In contrast, for in-plane field, the $H_{c2}^\parallel - T_C$ dependence near T_{C0} in the monolayer is much steeper than in the bulk and follows a square-root instead of a linear dependence. More significantly, the monolayer upper critical field H_{c20}^\parallel far exceeds its Pauli limit H_P while $H_{c20}^\parallel \gtrsim H_P$ in the bulk. We note that large enhancements of H_{c20}^\parallel ($\gg H_P$) have been observed in other systems^{9,27-31}. Many mechanisms have been discussed including strong coupling^{37,38}, modified electron g-factor^{19,30}, interaction effects³⁵⁻³⁷, remnant magnetic susceptibility at low temperature³⁰, Rashba SOI³⁰, and spin-orbit scattering from impurities^{27,28,31-34}. These effects, however, are insignificant in 2D NbSe₂^{11,12,37,39}. (See Supplementary Materials Section 6 for detailed discussions). In non-centrosymmetric monolayer NbSe₂, the large enhancement of H_{c20}^\parallel , as discussed above, can arise from the strong intrinsic SOIs and spin-momentum locking. In the absence of the orbital effect, H_{c20}^\parallel is determined by the alignment of spin by the external field. The upper critical field can be estimated by noting that the in-plane component of the spin magnetic moment is reduced to $\sim \frac{H_\parallel}{H_{SO}} \mu_B$ due to the competing SOI and Zeeman effect. Here $H_{SO} \equiv \frac{\Delta_{SO}}{\mu_B}$ is the effective magnetic field from the SOI with Δ_{SO} and μ_B denoting the spin-orbit splitting energy and the Bohr magneton, respectively. Pair breaking occurs when the effective Zeeman splitting energy $\sim \frac{H_\parallel^2}{H_{SO}} \mu_B$ overcomes the superconducting gap. It thus yields the following estimate for $H_{c20}^\parallel \sim \sqrt{H_{SO} H_P}$, which can greatly exceed H_P if $H_{SO} \gg H_P$ for strong SOIs.

To analyze the entire $H_{c2}^\parallel - T_C$ phase diagram, we introduce the pair breaking equation¹⁹ for monolayer NbSe₂ with the spin-momentum locking effect incorporated

$$\ln\left(\frac{T_C}{T_{C0}}\right) + \psi\left(\frac{1}{2} + \frac{\mu_B H_\parallel^2 / H_{SO}}{2\pi k_B T_C}\right) - \psi\left(\frac{1}{2}\right) = 0. \quad (1)$$

Here $\psi(x)$ is the digamma function and k_B is the Boltzmann constant. Near T_{C0} , Eqn. 1 can be reduced to $\left(1 - \frac{T_C}{T_{C0}}\right) = \frac{(H_{c2}^\parallel)^2}{H_{SO} H_P}$, which describes well the observed square-root dependence of $H_{c2}^\parallel \propto \sqrt{T_{C0} - T_C}$. We fit the experimental $H_{c2}^\parallel - T_C$ dependence to the solution of Eqn. 1 with H_{SO} as a free parameter. The best fit (blue line, fig. 4) gives the effective magnetic field $H_{SO} \approx 660$ T, or equivalently, the total spin splitting energy $2\Delta_{SO} \approx 76$ meV. This value agrees well with the values from *ab initio* calculations for the Fermi surface around the K and K' point of the Brillouin zone (~ 70 -80 meV)¹⁸, where effects of SOIs on Cooper pairing are the strongest. The upper critical field is determined from Eqn. 1 $H_{c20}^\parallel \approx 35$ T, which is over 6 times of H_P . To verify this value, we have performed independent differential conductance measurements of a monolayer

at 0.3 K up to $H_{\parallel} = 31.5$ T. (See Supplementary Materials section 7 for details.) A zero-bias peak originated from Andreev reflections at the normal metal-superconductor contact was observed. With increasing magnetic field, the zero-bias peak diminishes continuously, corresponding to a shrinking superconducting gap, and becomes very weak at 31.5 T (inset of Fig. 4). This result suggests that $H_{c20}^{\parallel} \gtrsim 31.5$ T, consistent with the result from Eqn. 1.

Finally, we briefly comment on the $H_{c2}^{\parallel} - T_c$ phase diagram for the few-layer and bulk sample. As N increases, interlayer-coupling kicks in, the orbital effect can quench superconductivity in addition to the spin effect, and the upper critical field H_{c20}^{\parallel} decreases. However, for layer thickness smaller than the out-of-plane penetration depth (~ 23 nm¹⁰), the orbital effect is strongly suppressed¹⁹ and similar $H_{c2}^{\parallel} - T_c$ dependences are observed for few-layer samples with $H_{c20}^{\parallel} > 3H_p$ in both bilayer and trilayer NbSe₂. The observation of $H_{c20}^{\parallel} \gg H_p$ in bilayer NbSe₂, which is centrosymmetric and for which spin-momentum locking is destroyed, suggests the importance of SOIs in bilayers as well. Indeed, as long as interlayer coupling does not cause spin-flip [demonstrated by spin polarized angle resolved photoemission spectroscopy (ARPES) in group-VI TMDs⁷], the out-of-plane spin is still a good quantum number. It is locked to each individual layer, known as spin-layer locking⁶, which also protects superconductivity under a parallel magnetic field. On the other hand, in the bulk limit, the orbital effect dominates the phase diagram as for the case of out-of-plane fields. The estimated in-plane upper critical field $H_{c20}^{\parallel} \approx 17$ T (from 70% of the linear extrapolation of the $H_{c2}^{\parallel} - T_c$ dependence at zero temperature⁴⁰), which is about 4 times higher than H_{c20}^{\perp} , is in good agreement with the reported value^{9,10}. We note that the above discussion on the magnetic response of few-layer samples is very qualitative. More detailed experimental and theoretical studies are warranted for a full understanding of the interplay between spin-layer locking and orbital effects, and of the importance of the complex Fermi surface of NbSe₂^{13,14}. Our studies on the strong SOIs and spin-momentum locking in atomically thin NbSe₂ down to the monolayer thickness open up a new avenue for the study of interacting electrons with Ising spin in the exact 2D limit.

References:

- 1 Xu, X., Yao, W., Xiao, D. & Heinz, T. F. Spin and pseudospins in layered transition metal dichalcogenides. *Nature Physics* **10**, 343-350 (2014).
- 2 Xiao, D., Liu, G.-B., Feng, W., Xu, X. & Yao, W. Coupled Spin and Valley Physics in Monolayers of MoS₂ and Other Group-VI Dichalcogenides. *Physical Review Letters* **108**, 196802 (2012).
- 3 Mak, K. F., He, K., Shan, J. & Heinz, T. F. Control of valley polarization in monolayer MoS₂ by optical helicity. *Nature Nanotechnology* **7**, 494-498 (2012).
- 4 Zeng, H., Dai, J., Yao, W., Xiao, D. & Cui, X. Valley polarization in MoS₂ monolayers by optical pumping. *Nature Nanotechnology* **7**, 490-493 (2012).

- 5 Mak, K. F., McGill, K. L., Park, J. & McEuen, P. L. The valley Hall effect in MoS₂ transistors. *Science* **344**, 1489-1492 (2014).
- 6 Jones, A. M. *et al.* Spin-layer locking effects in optical orientation of exciton spin in bilayer WSe₂. *Nature Physics* **10**, 130-134 (2014).
- 7 Riley, J. M. *et al.* Direct observation of spin-polarized bulk bands in an inversion-symmetric semiconductor. *Nature Physics* **10**, 835-839 (2014).
- 8 Mattheiss, L. F. Band structures of transition-metal-dichalcogenide layer compounds. *Physical Review B* **8**, 3719-3740 (1973).
- 9 Foner, S. & McNiff, E. J. Upper critical fields of layered superconducting NbSe₂ at low-temperatures. *Physics Letters A* **45**, 429-430 (1973).
- 10 Trey, P. D., Gygax, S. & Jan, J. P. Anisotropy of Ginzburg-Landau parameter κ in NbSe₂. *Journal of Low Temperature Physics* **11**, 421-434 (1973).
- 11 Hess, H. F., Robinson, R. B., Dynes, R. C., Valles, J. M. & Waszczak, J. V. Scanning-tunneling-microscope observation of the Abrikosov flux lattice and the density of states near and inside a fluxoid. *Physical Review Letters* **62**, 214-216 (1989).
- 12 Huang, C. L. *et al.* Experimental evidence for a two-gap structure of superconducting NbSe₂: A specific-heat study in external magnetic fields. *Physical Review B* **76**, 212504 (2007).
- 13 Yokoya, T. *et al.* Fermi surface sheet-dependent superconductivity in 2H-NbSe₂. *Science* **294**, 2518-2520 (2001).
- 14 Rahn, D. J. *et al.* Gaps and kinks in the electronic structure of the superconductor 2H-NbSe₂ from angle-resolved photoemission at 1 K. *Physical Review B* **85**, 224532 (2012).
- 15 Frindt, R. F. Superconductivity in ultrathin NbSe₂ layers. *Physical Review Letters* **28**, 299 (1972).
- 16 Staley, N. E. *et al.* Electric field effect on superconductivity in atomically thin flakes of NbSe₂. *Physical Review B* **80**, 184505 (2009).
- 17 Xiaoxiang Xi *et al.* Strongly enhanced charge-density-wave order in monolayer NbSe₂. *Nature Nanotechnology* 10.1038/nnano.2015.143 (2015).
- 18 Johannes, M. D., Mazin, I. I. & Howells, C. A. Fermi-surface nesting and the origin of the charge-density wave in NbSe₂. *Physical Review B* **73**, 205102 (2006).
- 19 Tinkham, M. *Introduction to superconductivity*. 2nd edn, (McGraw-Hill, 1996).
- 20 Chandrasekhar, B. S. A note on the maximum critical field of high-field superconductors. *Applied Physics Letters* **1**, 1777362 (1962).
- 21 Clogston, A. M. Upper limit for critical field in hard superconductors. *Physical Review Letters* **9**, 266 (1962).
- 22 Fiory, A. T. & Hebard, A. F. Electron-mobility, conductivity, and superconductivity near the metal-insulator-transition. *Physical Review Letters* **52**, 2057-2060 (1984).
- 23 Beasley, M. R., Mooij, J. E. & Orlando, T. P. Possibility of vortex-antivortex pair dissociation in 2-dimensional superconductors. *Physical Review Letters* **42**, 1165-1168 (1979).
- 24 Aslamazov, L. G. & Larkin, A. I. Influence of fluctuation pairing of electrons on conductivity of normal metal. *Physics Letters A* **26**, 238 (1968).

- 25 Li, Q. *et al.* Interlayer coupling effect in high-Tc superconductors probed by YBa₂Cu₃O_{7-x}/PrBa₂Cu₃O_{7-x} superlattices. *Physical Review Letters* **64**, 3086-3089 (1990).
- 26 Schneider, T., Gedik, Z. & Ciraci, S. Transition-temperature of superconductor-insulator superlattices. *Europhysics Letters* **14**, 261-266 (1991).
- 27 Prober, D. E., Schwall, R. E. & Beasley, M. R. Upper critical fields and reduced dimensionality of the superconducting layered compounds. *Physical Review B* **21**, 2717-2733 (1980).
- 28 Tedrow, P. M. & Meservey, R. Critical magnetic-field of very thin superconducting aluminum films. *Physical Review B* **25**, 171-178 (1982).
- 29 Lee, I. J., Chaikin, P. M. & Naughton, M. J. Exceeding the Pauli paramagnetic limit in the critical field of (TMTSF)₂PF₆. *Physical Review B* **62**, 14669-14672 (2000).
- 30 E. Bauer & Sigrist, M. *Non-centrosymmetric Superconductors: Introduction and Overview* 40 (Springer-Verlag, 2012).
- 31 Klemm, R. A. *Layered Superconductors* Vol. 1 (Oxford University Press, 2012).
- 32 Maki, K. Effect of Pauli paramagnetism on magnetic properties of high-field superconductors. *Physical Review* **148**, 362 (1966).
- 33 Werthame, N. R., Helfand, E. & Hohenber, P. C. Temperature and purity dependence of superconducting critical field H_{c2}: 3. Electron spin and spin-orbit effects. *Physical Review* **147**, 295 (1966).
- 34 Klemm, R. A., Luther, A. & Beasley, M. R. Theory of upper critical-field in layered superconductors. *Physical Review B* **12**, 877-891 (1975).
- 35 Orlando, T. P. & Beasley, M. R. Pauli limiting and the possibility of spin fluctuations in the A15 superconductors. *Physical Review Letters* **46**, 1598-1601 (1981).
- 36 Matsuda, Y. & Shimahara, H. Fulde-Ferrell-Larkin-Ovchinnikov state in heavy fermion superconductors. *Journal of the Physical Society of Japan* **76**, 051005 (2007).
- 37 Agosta, C. C. *et al.* Experimental and semiempirical method to determine the Pauli-limiting field in quasi-two-dimensional superconductors as applied to kappa-(BEDT-TTF)₂Cu(NCS)₂: Strong evidence of a FFLO state. *Physical Review B* **85**, 214514 (2012).
- 38 Rainer, D. & Bergmann, G. Temperature-dependence of H_{c2} and K₁ in strong coupling superconductors. *Journal of Low Temperature Physics* **14**, 501-519 (1974).
- 39 MacNeill, D. *et al.* Breaking of valley degeneracy by magnetic field in monolayer MoSe₂. *Physical Review Letters* **114**, 037401 (2015).
- 40 D. Saint-James, G. Sarma & Thomas, E. J. *Type II Superconductivity*. (Pergamon, 1969).

Acknowledgments: We thank Moses H. W. Chan for fruitful discussions.

Methods:

Sample preparation and device fabrication. High-quality 2H-NbSe₂ single crystals were grown from Nb metal wires of 99.95% purity and Se pellets of 99.999% purity by iodine 99.8% vapor transport in a gradient of 730 °C – 700 °C in a sealed quartz tubes for 21 days. A very slight excess of Se was introduced (typically 0.2% of the charge) to ensure stoichiometry in the resulting crystals. Thin flakes were mechanically exfoliated from bulk single crystals on silicone elastomer polydimethylsiloxane (PDMS) stamps. Atomically thin samples of good geometry were first identified by optical microscopy and then transferred onto silicon substrates (covered by a 280 nm layer of thermal oxide) with pre-patterned Au electrodes. To minimize the environmental effects on the samples, we have limited their exposure to air to < 1 hour. Hexagonal boron nitride (h-BN) thin films of 10 – 20 nm thickness were introduced as a capping layer for further protection. The sample thickness was determined according to their shear mode frequency by Raman spectroscopy¹⁷. The crystal quality was characterized by polarized optical second harmonic generation. (See Supplementary Materials Section 1 for more details).

Electrical characterization. Transport and magneto-transport measurements were carried out in a Physical Property Measurement System (PPMS) down to 2.1 K and up to 9 T. For higher magnetic field measurements up to 31.5 T, a Janis He3 cryostat with base temperature of 0.3 K was employed. Unless specifically mentioned, longitudinal electrical resistance was acquired using a four-point geometry with excitation current limited to 1 μ A to avoid heating and high-bias effects. (Dependence on the excitation current was performed to study the fluctuation effects in 2D.) The devices were mounted on a rotation stick, which allows alignment of the sample plane with the external magnetic field with high accuracy (< 0.5° error). Multiple devices were prepared and measured. All yielded consistent results for samples of the same thickness.

Figures and Figure Captions:

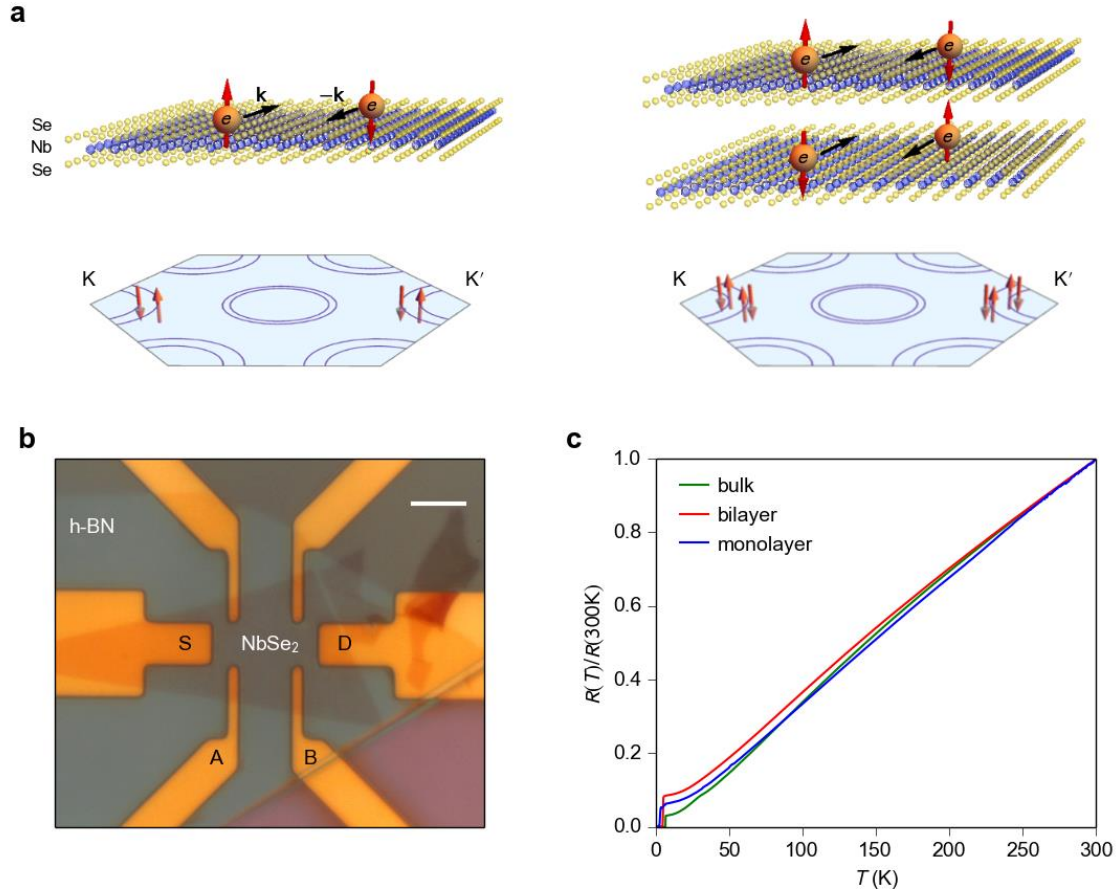


Fig. 1 Spin-momentum and spin-layer locking in NbSe₂. (a) Schematic illustration of spin-momentum locking in monolayer (left) and spin-layer locking in bilayer/bulk (right) NbSe₂. First row: Monolayer NbSe₂ consists of a layer of Nb atoms (blue balls) sandwiched between two layers of Se atoms (yellow balls) in the trigonal prismatic structure. Bulk 2H-NbSe₂ is made of monolayers stacked in the ABAB... sequence. Second row: Brillouin zone (BZ) in the in-plane direction and Fermi surface near the Γ , K and K' point. The Fermi surface is spin split in the monolayer and spin degenerate in the bilayer/bulk. (b) Optical image of a bilayer NbSe₂ device capped by a thin h-BN layer for environmental protection. The scale bar corresponds to 5 μm . Current was excited through electrode S and D; voltage drop was measured across A and B. (c) Temperature dependence of the normalized four-point resistance R for a typical bulk, bilayer and monolayer NbSe₂ device from 2.1 – 300 K.

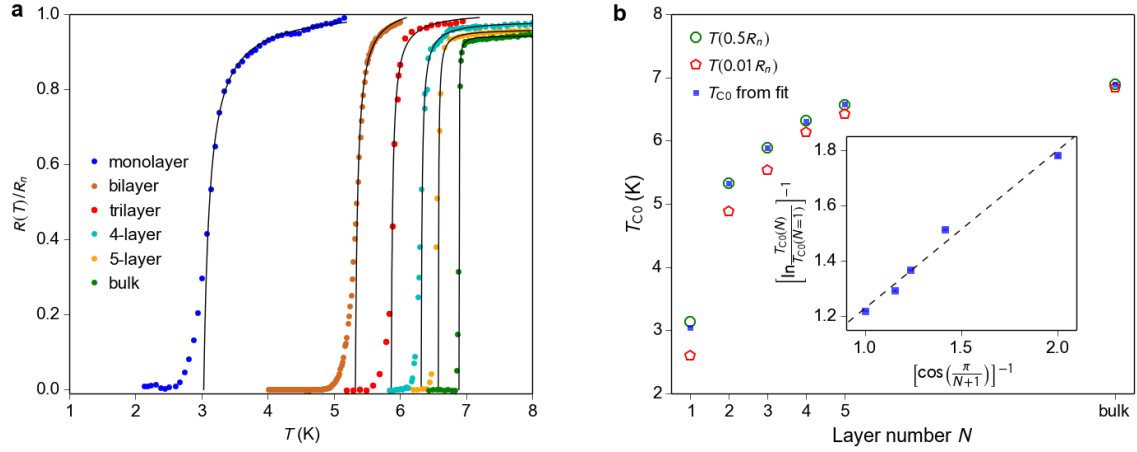


Fig. 2 Layer number dependence of superconductivity in NbSe₂. (a) Temperature dependence of the resistance for NbSe₂ samples of varying thickness. The resistance is normalized to the normal state value right above the superconducting transition. The solid lines are fits to the Aslamasov-Larkin formula for $R(T)/R_n > 0.5$. (b) Layer number N dependence of $T(0.5R_n)$, $T(0.01R_n)$, and T_{C0} . The inset shows the dependence of $\left[\ln \frac{T_{C0}(N)}{T_{C0}(N=1)}\right]^{-1}$ on $\left[\cos\left(\frac{\pi}{N+1}\right)\right]^{-1}$ (symbols), where $T_{C0}(N=1) \approx 3.0$ K. Dashed line is the best fit to a linear dependence.

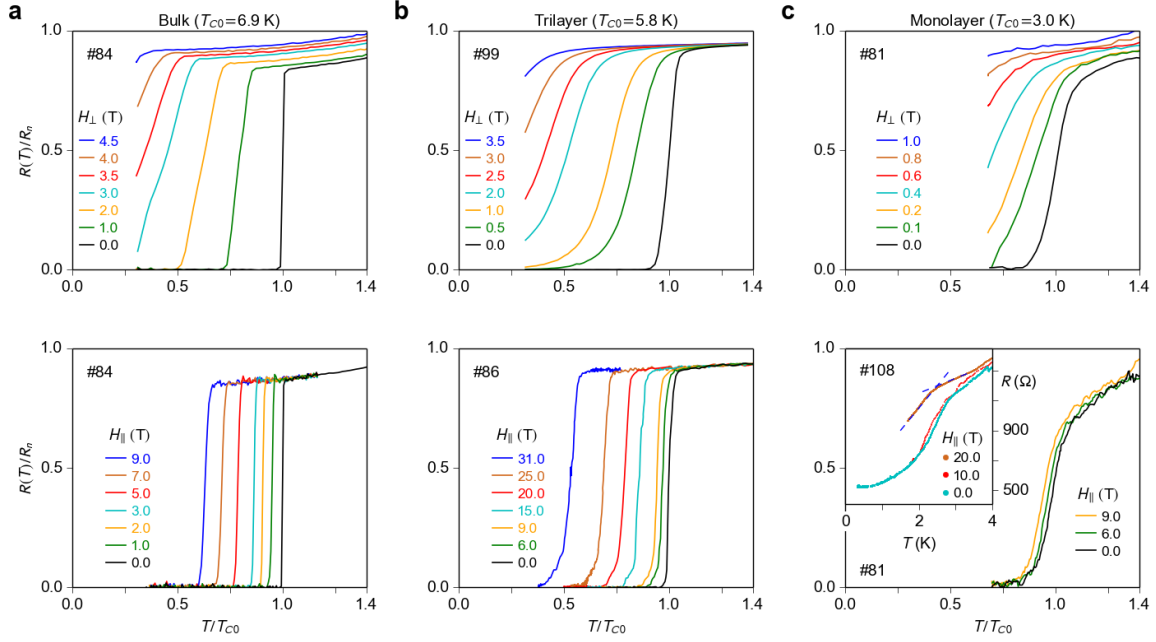


Fig. 3 Superconductivity of bulk, trilayer, and monolayer NbSe₂ under a magnetic field. Temperature dependence of the dc resistance for a bulk (a), trilayer (b), and monolayer NbSe₂ device (c) under out-of-plane (H_{\perp}) and in-plane (H_{\parallel}) magnetic fields. The inset to (c) shows the two-point resistance of second monolayer device under in-plane magnetic fields. The crossing of the two dashed lines is used to determine T_C .

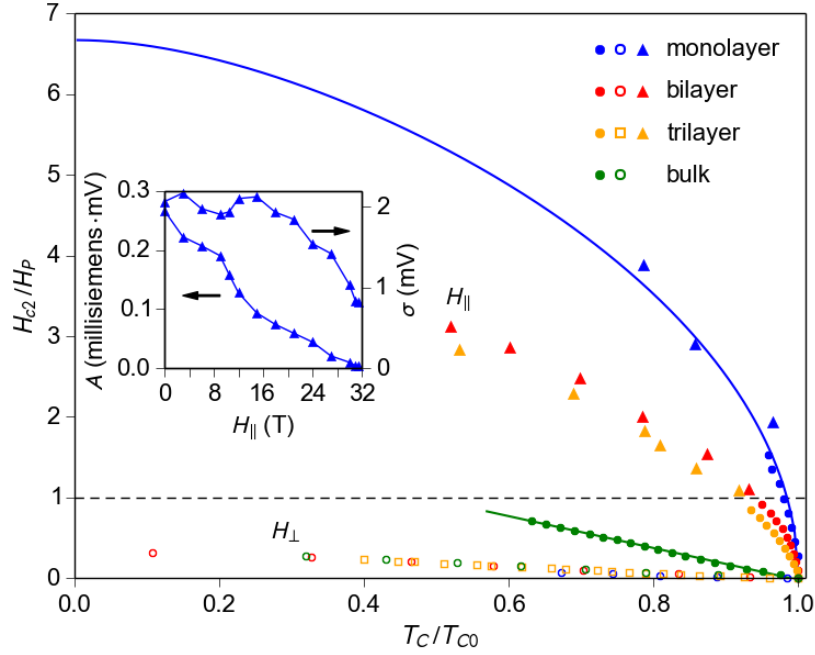


Fig. 4 $H - T$ superconducting phase diagram for atomically thin NbSe₂. The critical field H_{c2}/H_P as a function of transition temperature T_C/T_{C0} is shown for NbSe₂ samples of differing thickness under both out-of-plane H_{\perp} (open symbols) and in-plane H_{\parallel} (filled symbols) magnetic fields. The dashed line corresponds to the Pauli paramagnetic limit H_P . The blue line is the best fit to the solution of the pair breaking equation. The green line is a linear fit. The inset shows the zero-bias peak area and width as a function of H_{\parallel} at 0.36 K obtained from differential conductance measurements in a monolayer device. The result shows that superconductivity in monolayer NbSe₂ survives under $H_{\parallel} = 31.5$ T.